SCIENTIFIC REPORTS

OPEN

SUBJECT AREAS:
ELECTRONIC PROPERTIES AND MATERIALS
SUPERCONDUCTING PROPERTIES AND MATERIALS

Received
8 August 2013

Accepted
24 February 2014

Published
14 March 2014

Correspondence and requests for materials should be addressed to M.S. (sc20217@s.okayama-u.ac.jp) or T.Y. (yokoya@cc.okayama-u.ac.jp)

Characteristic two-dimensional Fermi surface topology of high-T_c iron-based superconductors

Masanori Sunagawa[1,2], Toshihiko Ishiga[1,2], Koji Tsubota[1,2], Taihei Jabuchi[1,2], Junki Sonoyama[1,2], Keita Iba[1,3], Kazutaka Kudo[1,3], Minoru Nohara[1,3], Kanta Ono[4], Hiroshi Kumigashira[4], Tomohiro Matsushita[5], Masashi Arita[6], Kenya Shimada[6], Hirofumi Namatame[6], Masaki Taniguchi[6], Takanori Wakita[1,2], Yuji Muraoka[1,2] & Takayoshi Yokoya[1,2]

[1]The Graduate School of Natural Science and Technology, Okayama University, Okayama 700-8530, Japan, [2]Research Laboratory for Surface Science, Okayama University, 3-1-1 Tsushima-naka, Okayama 700-8530, Japan, [3]Department of Physics, Okayama University, Okayama 700-8530, Japan, [4]Institute for Material Structure Science, High Energy Accelerator Research Organization, Tsukuba, Ibaraki 305-0801, [5]Japan Synchrotron Radiation Research Institute (JASRI)/SPring-8, 1-1-1 Kouto, Sayo, Hyogo 679-5198, Japan, [6]Hiroshima Synchrotron Radiation Center, Hiroshima University, Higashi-Hiroshima, Hiroshima 739-0046, Japan.

Unconventional Cooper pairing originating from spin or orbital fluctuations has been proposed for iron-based superconductors. Such pairing may be enhanced by quasi-nesting of two-dimensional electron and hole-like Fermi surfaces (FS), which is considered an important ingredient for superconductivity at high critical temperatures (high-T_c). However, the dimensionality of the FS varies for hole and electron-doped systems, so the precise importance of this feature for high-T_c materials remains unclear. Here we demonstrate a phase of electron-doped $CaFe_2As_2$ (La and P co-doped $CaFe_2As_2$) with $T_c = 45$ K, which is the highest T_c found for the $AEFe_2As_2$ bulk superconductors (122-type; AE = Alkaline Earth), possesses only cylindrical hole- and electron-like FSs. This result indicates that FS topology consisting only of two-dimensional sheets is characteristic of both hole- and electron-doped 122-type high-T_c superconductors.

Iron-based superconductors are considered to be important for understanding high temperature superconductivity from a new perspective due to the presence of a high superconducting critical temperature (T_c) that cannot be explained within the framework of conventional phonon-mediated BCS superconductivity. Moreover, the electronic states of the parent compounds and the superconducting symmetry in these systems are different from those for high-T_c cuprate superconductors[1–3]. Spin fluctuation-mediated superconductivity, as proposed for cuprate and heavy fermion systems, and orbital fluctuation-mediated superconductivity have been proposed as mechanisms for superconductivity[4–7]. Such fluctuations are believed to be derived from the quasi-nesting between the hole- and electron-like Fermi surfaces (FSs) (Fig. 1a). There is much discussion surrounding the relevance of the FS topology to iron-based superconductivity.

In order to clarify the relevance of the Fermi surface to the mechanism of superconductivity in iron-based superconductors from an experimental perspective, numerous angle-resolved photoemission spectroscopy (ARPES) measurements, which are a direct measurement of the Fermi surface, have been conducted on iron-based superconductors[8–27]. A number of substances with $T_c > 50$ K have been discovered for REFeAsO (1111-type; RE = Rare Earth) superconductors[28], which has drawn corresponding interest in the electronic structures that manifest such high values of T_c. However, few ARPES measurements have been performed in these materials, due to the difficulty in fabricating single crystals of large dimensions[8–10]. In addition, bulk band structures are difficult to determine due to substantial surface effects originating from the existence of the REO layers[10]. As a result, little is known about the Fermi surface topology in the 1111-type materials. In contrast, numerous ARPES measurements have been performed for $AEFe_2As_2$ (122-type; AE = Alkaline Earth) iron-based superconductors[17–27], which do not possess REO layers. ARPES measurements are more feasible for this system due to the availability of larger single crystals and the lack of surface effects associated with REO layers. ARPES experiments in the 122 system are thus believed to more closely reflect bulk electronic structure. ARPES studies in the 122 system reveal the presence of hole-like and electron-like Fermi surfaces at the center of the Brillouin zone and the

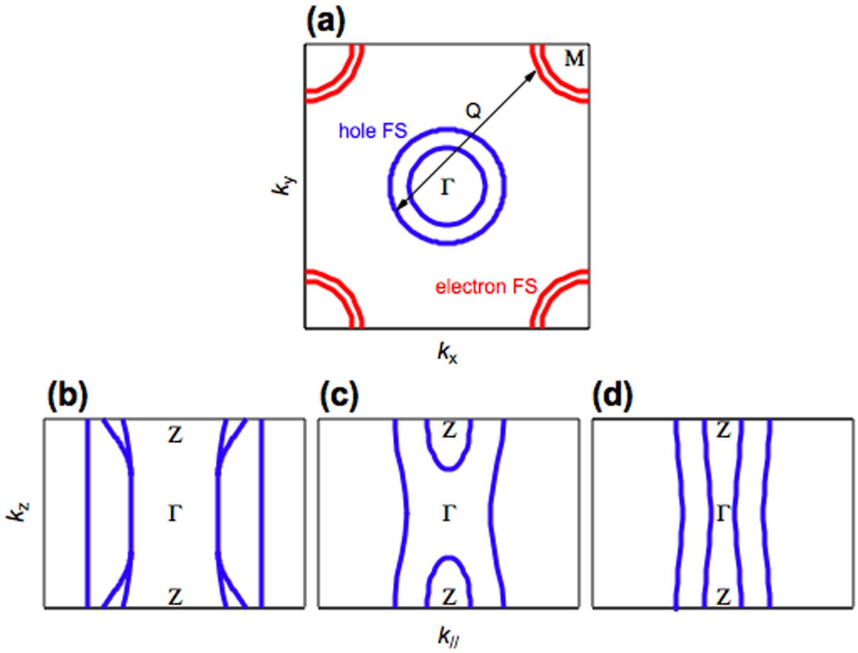

Figure 1 | Schematic Fermi surface topology. (a) Sketch of the band calculation results of Refs. 4 and 5, illustrating the Fermi surface (FS) and the nesting with nesting vector Q in the k_x-k_y plane for iron-based superconductors. The red and blue curved lines indicate electron- and hole-like FSs, respectively. (b) and (c) Sketch of the ARPES results of Refs. 24 and 26, illustrating the hole-like FSs around the zone center in the k_z–$k_{//}$ plane for $Ba_{1-x}K_xFe_2As_2$ and $Ba(Fe_{1-x}Co_x)_2As_2$. (d) Sketch of the present ARPES results for $Ca_{0.82}La_{0.18}Fe_2(As_{0.94}P_{0.06})_2$.

corner, respectively, and the cylindrical shape of the electron-like Fermi surfaces at the zone corner are common features of the electronic structure in high-T_c 122-type superconductors.

However, as shown in Fig. 1b and 1c, the shape of the Fermi surface at the zone center varies depending on the particular compound. The k_z dispersion is weak for the hole-doped 122-type $Ba_{1-x}K_xFe_2As_2$ (T_c = 38 K) and so the FSs is nearly two-dimensional[24,25]. However, FSs with strongly three-dimensional oval shapes exist in the vicinity of the zone center for $Ba(Fe_{1-x}Co_x)_2As_2$ (T_c = 25 K)[26,27]. Two-dimensional FSs, which are more conducive to nesting, are considered to be linked to the emergence of high-T_c in iron-based superconductors. However, since the FS dimensionality varies for these two iron-based superconductors with high-T_c, the importance of a two-dimensional Fermi surface topology is unclear.

An electron-doped $CaFe_2As_2$ superconductor derived by co-doping La and P was recently discovered with T_c = 45 K[29]. The T_c of this new iron-based superconductor is the highest among the 122-type bulk superconductors that have ever been studied with ARPES. Thus, it is important to study the electronic structure using ARPES to clarify the FS topology of the iron-based superconductors at such a high T_c.

In our study, we revealed the Fermi surface of the electron-doped $CaFe_2As_2$. ARPES measurements were conducted with three photon polarizations to resolve multiple bands and tunable excitation photon energy to observe the three-dimensional shape of the Fermi surfaces (k_z dispersion of Fermi surfaces). All Fermi surfaces of this new superconductor had a weak k_z dispersion. Since this characteristic is common to $Ba_{1-x}K_xFe_2As_2$, which has the maximum T_c among hole-doped 122-type superconductors, the two-dimensional topology of the Fermi surface is relevant to the presence of high T_c in the iron-based superconductors and does not rely on the character of doped carriers.

Results

Polarization and photon energy dependent ARPES. In Fig. 2a–f, we show polarization dependent ARPES intensity plots (for the geometrical measurement configuration, see Supplementary Fig. S1) along the cuts passing through the Γ point ($h\nu$ = 31 eV) and the Z point ($h\nu$ = 19 eV), together with peak positions determined from energy distribution curve (EDC) and momentum distribution curve (MDC) analyses (See, Supplementary Fig. S2 and S3 for corresponding intensity plots, intensity plots normalized with the Fermi-Dirac distribution function, and selected MDCs and EDCs.). At both points, ARPES intensity plots exhibit marked polarization dependence, which enables us to distinguish the dispersions of the three bands. At the Γ point, using ARPES data for *s*-polarized (*s*-pole) light (Fig. 2b, S2e–h), we found an intense hole-like dispersion with an energy maximum around 25 meV (α_1). The multiple structure of MDC at E_F (and its detailed line shape analysis) (Fig. S2g) also indicates the existence of E_F crossings of another band (α_2). In ARPES data for circular-polarized (*c*-pole) light (Fig. 2a, S2a–d), we found that the hole-like band (α_2) approaches and crosses E_F, as evident from multiple structures in the MDC at E_F (and its detailed line shape analysis) (Fig. S2c) and the parabolic dispersion in the EDCs (Fig. S2d). In addition, we found a hole-like feature (β) crossing E_F outside of the α_2 band in ARPES data for *p*-polarized (*p*-pole) light (Fig. 2c, S2i–k), which is more easily observed in MDCs for a higher binding energy region (Fig. S2k). At the Z point, while the intense hole-like α_1 band with an energy maximum around 10 meV is similarly found in *s*-pole data (Fig. 2e, S3d–f), the β band is observed in *c*- and *p*-pole data (Fig. 2d and 2f, S3a–c and S3g–h). Although intensities of the α_2 band are weaker than that of the β band at the Z point ($h\nu$ = 19 eV), the existence of k_Fs can be confirmed by the multiple structure in the MDC at E_F (and its detailed line shape analysis) taken with $h\nu$ = 82 eV, which corresponds to another Z point (Supplementary Figs. S3i–k). These data and analyses confirm the existence of three bands consistent with band structure calculations[4,5].

Having established the existence of three bands, we now examine the k_z dispersion of the bands from photon energy-dependent ARPES. The peak positions of the normal emission spectra in Fig. 2h, corresponding to α_1, measured with various photon energies

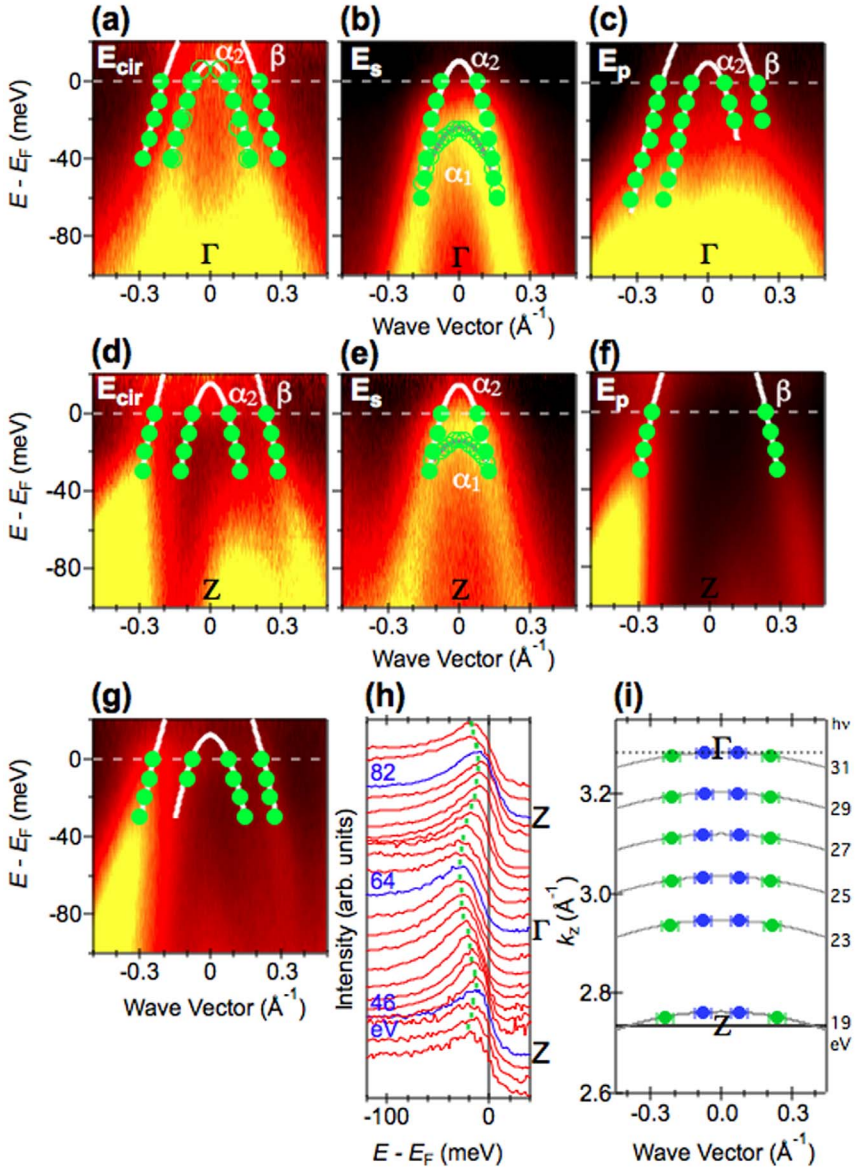

Figure 2 | Polarization and photon energy dependent ARPES data for $Ca_{0.82}La_{0.18}Fe_2(As_{0.94}P_{0.06})_2$ near the zone center. (a)–(c) ARPES intensity plots taken at $h\nu = 31$ eV ($k_z \sim \Gamma$) with circular (E_{cir}), s (E_s) and p (E_p) polarizations. (d)–(f) are the same as (a)–(c) but taken at $h\nu = 19$ eV ($k_z \sim$ Z). (g) ARPES intensity plot taken at $h\nu = 23$ eV with circular polarization. In (a)–(g), intensities are divided by the Fermi-Dirac function. Filled and open circles denote peak positions determined from analyses of the MDCs and EDCs, respectively. (h) The EDCs divided by the Fermi-Dirac function at $k_{||} = 0$ measured with various photon energies. (i) The k_Fs determined from the MDC analysis shown in Supplementary Figure S5.

show a periodic variation consistent with the periodicity of the bulk Brillouin zone. More importantly, the peak positions are located below E_F for all k_zs measured, indicating that this band does not contribute to the FS. For α_2 and β, we found that hole-like Fermi surfaces are formed at both Γ and Z points. ARPES data at hν = 23 eV, corresponding to k_z between Γ and Z, also shows E_F crossings of these bands (Fig. 2g and S4a–d). We found that photon energy-dependent MDCs at E_F for the [100] direction near the zone center can be well reproduced with four Lorentzian functions (Supplementary Fig. S5). We plotted the k_Fs determined from fitting the MDCs at E_F in Fig. 2i. We now find that the α_2 and β bands form a nearly cylindrical small and large hole-like FS, respectively.

In Fig. 3a and 3b, ARPES intensity plots at E_F as functions of the two-dimensional wave vectors (k_x, k_y) around the M and A point, respectively, together with the positions of k_F (filled circles) obtained from fits to the MDC are shown. We observed two electron-like FSs. These FSs originate from the inner ε and outer δ electron-like bands, as shown in Fig. 3c and 3d. We identified these bands from the detailed analysis of the MDCs (Supplementary Fig. S6a and S6b). We separate the two electron-like bands at the A point by performing polarization dependent ARPES taken at $h\nu = 24$ eV, which corresponds to another A point (Supplementary Fig. S6c and S6d). The elliptical shape of the intersections of the inner ε and outer δ electron-like FSs rotates 90° from M to A, which is consistent with the shape of the boundary of the body-centered tetragonal Brillouin zone. In Fig. 3e, we show the results of the FS mapping in the $k_{||}$-k_z plane near the zone corner. The direction of $k_{||}$ is the same as the cuts in Fig. 3a and 3b. The electron-like FSs show a sizeable undulation along the k_z direction (Fig. 3e), reflecting the elliptical shape of these FSs and the shape of the zone boundary, as described above.

The Fermi surface topology determined by ARPES. From these ARPES measurements, we draw the shape of the FSs corresponding to the observed bands crossing E_F (α_2, β, ε, δ), as shown in Fig. 4a

and 4b. We now find four FSs: two around the zone center derived from the hole-like bands (α_2, β) and two around the zone corner derived from the electron-like bands (ε, δ). All the FSs around the zone center and the corner are found to be nearly cylindrical with a small undulation. Here, hole-like FSs shifted by the AFM wave vector (π/a, π/a, $2\pi/c$) of $CaFe_2As_2$[30,31], where a = 3.914 Å and c = 11.48 Å are the in-plane and out-of-plane lattice constants of $Ca_{0.82}La_{0.18}Fe_2(As_{0.94}P_{0.06})_2$, are shown with broken blue and sky blue lines in Fig. 4a. Some values for k_F of the inner ε electron-like FS overlap with those of the shifted β FS. Note that the back folding of the bands, which has been observed in the 122-type parent compounds[32] and $Ca_{0.83}La_{0.17}Fe_2As_2$ with trace superconductivity[33], is absent in the present compound, consistent with the absence of AFM ordering. The total hole and electron count from the observed FS yields a hole volume of 6 ± 2% and an electron volume of 18 ± 5%. Here, we assume that the hole-like parts of the FS are circular. The deduced total carrier number of 0.12 ± 0.07 electrons per Fe is consistent with the value of 0.09 electrons per Fe expected from the chemical composition, indicating that our measurements reflect the observation of the bulk electronic structure of La and P co-doped $CaFe_2As_2$.

Discussion

We discuss the implication of the present ARPES results for iron-based superconductivity. As shown in Fig. 1b and 1d, all hole-like FSs in hole-doped $Ba_{1-x}K_xFe_2As_2$ and electron-doped $Ca_{0.82}La_{0.18}Fe_2(As_{0.94}P_{0.06})_2$ have a nearly two-dimensional shape[24,25]. We find that a two-dimensional FS topology, which favors electron pair scattering between quasi-nested FSs, is universal for high-T_c superconductivity regardless of the type of doped carrier. This observation supports the exotic pairing mechanisms proposed for iron-pnictide superconductors. Here it is noted that the quasi-nesting between hole- and electron-like FSs would not explain the high T_c of $K_xFe_{1-y}Se_2$ superconductors where hole-like FSs are absent[14–16].

One of the most important questions is the origin of high-T_c superconductivity in the electron-doped superconductor $Ca_{0.82}La_{0.18}Fe_2(As_{0.94}P_{0.06})_2$ (T_c = 45 K). We shall discuss the FS topology in three-dimensional momentum space. As described above, the size of the β hole-like FS is nearly the same as that of the ε electron-like FS and both FSs have a weak k_z dispersion, giving rise to a partial overlapping of k_Fs. These observations are similar to that for electron-doped $Ba(Fe_{1-x}Co_x)_2As_2$ (T_c = 25 K)[22]. An observable difference between $Ca_{0.82}La_{0.18}Fe_2(As_{0.94}P_{0.06})_2$ and $Ba(Fe_{1-x}Co_x)_2As_2$ in terms of FS topology is the dimensionality of the inner hole-like FS, as shown Fig. 1c and 1d. For $Ba(Fe_{1-x}Co_x)_2As_2$, the inner hole-like FS shows a strong k_z dispersion and is closed near the Γ point[25,26]. In contrast, the inner hole-like FS (α_2) shows a cylindrical shape and survives near the Γ point in $Ca_{0.82}La_{0.18}Fe_2(As_{0.94}P_{0.06})_2$. These results suggest that an enhancement of the two-dimensionality of the inner hole-like FS induces a large T_c difference in the two materials, possibly due to an increased

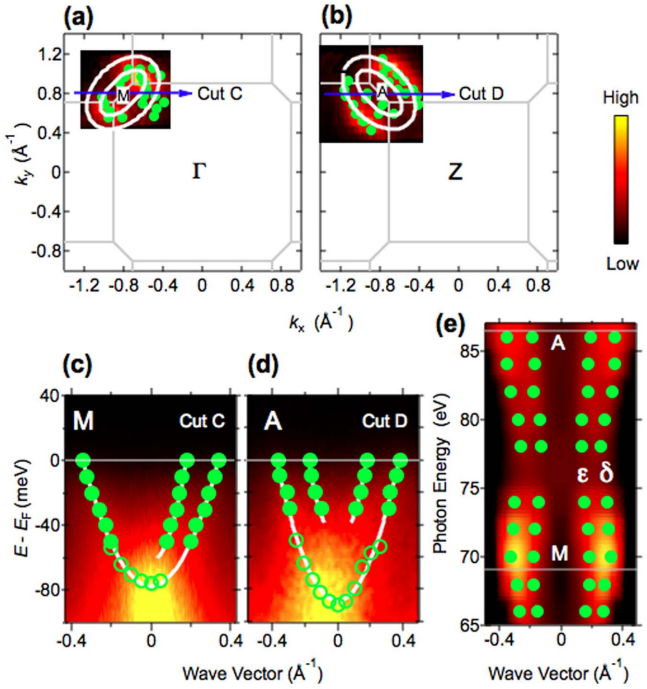

Figure 3 | Photon energy-dependent ARPES data for $Ca_{0.82}La_{0.18}Fe_2(As_{0.94}P_{0.06})_2$ around the zone corner. (a),(b) ARPES intensity plots at E_F as functions of two-dimensional wave vectors taken at $h\nu$ = 69 eV and $h\nu$ = 86 eV, respectively, around M and A. (c),(d) ARPES intensity plots along cuts C and D, respectively. Cuts C and D are shown by blue arrows in (a) and (b). In these plots, $k_{||}$ = 0 corresponds to the (π,π) point. Filled and open circles indicate the peak position of the MDCs and EDCs, respectively. (e) ARPES intensity plot at E_F as a function of photon energy, together with k_Fs (green dots) determined from the MDC analysis. The direction of $k_{||}$ is the same as (c) and (d) ([100] direction). The intensities are symmetrized about the $k_{||}$ = 0. In this plot, $k_{||}$ = 0 also corresponds to (π,π) point.

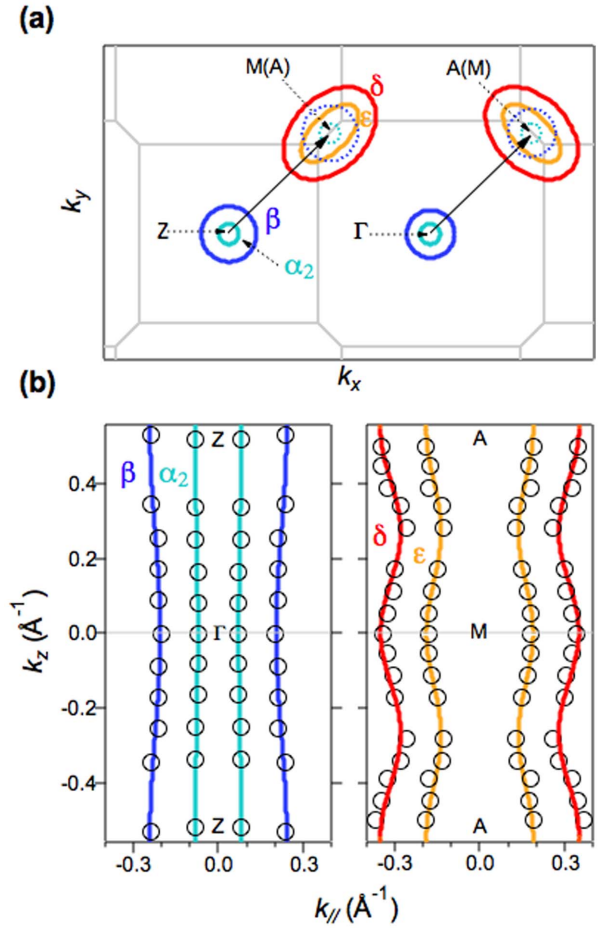

Figure 4 | Fermi surface shape for $Ca_{0.82}La_{0.18}Fe_2(As_{0.94}P_{0.06})_2$ determined by ARPES. The shapes of Fermi surfaces (FSs) in the (a) k_x-k_y and (b) k_z–$k_{||}$ planes are drawn with lines. Dotted blue and sky blue lines in (a) are two hole-like FSs around the zone center shifted by the antiferromagnetic vector (black arrows). In (b), black open circles represent experimentally determined k_Fs from photon energy-dependent ARPES. The positions of k_F have been symmetrized with respect to the symmetry lines.

tendency toward quasi-nesting between α_2 and ε parts of the FS. Regarding the orbital character of the bands in $Ca_{0.82}La_{0.18}Fe_2(As_{0.94}P_{0.06})_2$, the polarization dependence of the odd symmetry with respect to the mirror plane and k_z dispersion of α_1 enable us to suggest a d_{YZ} character for α_1, where X and Y refer to the direction rotated by 45 degrees from the Fe-Fe direction and Z is normal to the XY plane. The observable ARPES intensity of the α_2 band with both *s*-pole and *p*-pole light (Fig. 2a–c) suggests a mixed orbital character of even and odd symmetry. The mixed orbital character of bands near E_F (d_{XY} and d_{X2-Y2}) were reported from polarization dependent ARPES of $Ba(Fe_{1-x}Co_x)_2As_2$ and LiFeAs[11,19]. The β band has even symmetry. The lifting of the hole-like band degeneracy at the Γ point does not agree with previous calculations[4,5], where bands with d_{XZ} and d_{YZ} orbital characters are degenerate. However, recent calculations in Refs. 34 and 35 taking into account the change of the Fe-As-Fe bond angle and the change of the positive charge in the blocking layer predicted the lift of the degeneracy, in agreement with the present study.

In iron-based superconductors, band structure calculations predict that the shapes of the hole-like FSs become more three-dimensional with a reduction in pnictogen height[36]. This theoretical prediction holds for $Ba(Fe_{1-x}Co_x)_2As_2$ and $Ba_{1-x}K_xFe_2As_2$, as the pnictogen height of $Ba(Fe_{1-x}Co_x)_2As_2$ is shorter than that of $Ba_{1-x}K_xFe_2As_2$[37,38]. For $Ca_{0.82}La_{0.18}Fe_2(As_{0.94}P_{0.06})_2$, the pnictogen height is not available thus far. As for the *c* parameter, that of $Ca_{0.82}La_{0.18}Fe_2(As_{0.94}P_{0.06})_2$ is the shortest among the three compounds. However, this does not necessarily mean a shorter pnictogen height in $Ca_{0.82}La_{0.18}Fe_2(As_{0.94}P_{0.06})_2$, due to the difference in alkaline earths. In order to verify this relationship, detailed structural studies of $Ca_{0.82}La_{0.18}Fe_2(As_{0.94}P_{0.06})_2$ are indispensable.

In summary, we have investigated the three-dimensional electronic structure near E_F in electron-doped $Ca_{0.82}La_{0.18}Fe_2(As_{0.94}P_{0.06})_2$ (T_c = 45 K). The observed FS topology is nearly two-dimensional and similar to that of $Ba_{1-x}K_xFe_2As_2$, indicating the existence of universality in the FS topology for realizing high-T_c in 122-type superconductors.

Methods

High quality $Ca_{0.82}La_{0.18}Fe_2(As_{0.94}P_{0.06})_2$ single crystals were grown as described elsewhere[25]. Polarization dependent ARPES measurements ($h\nu$ = 19–31 eV) were carried out at BL-9A of Hiroshima Synchrotron Radiation Center (HSRC). ARPES measurements using circularly polarized light ($h\nu$ = 40–86 eV) were carried out at BL-28A of the Photon Factory. The total energy resolution was set to 10–30 meV. Clean surfaces were obtained by *in situ* cleaving of the crystal in a working vacuum better than 3×10^{-8} Pa and measured at 60 K (above T_c). The inner potential was determined to be 14 eV from photon energy-dependent ARPES studies as described above. Calibration of E_F of the sample was achieved using a gold reference.

1. Ishida, K., Nakai, Y. & Hosono, H. To What Extent Iron-Pnictide New Superconductors Have Been Clarified: A Progress Report. *J. Phys. Soc. Jpn.* **78**, 062001 (2009).
2. Mazin, I. I. & Schmalian, J. Pairing symmetry and pairing state in ferropnictides: Theorical overview. *Physica C* **469**, 614 (2009).
3. Wang, Fa. & Lee, D.-H. The Electron-Pairing Mechanism of Iron-Based Superconductors. *Science* **332**, 200 (2011).
4. Mazin, I. I., Singh, D. J., Johannes, M. D. & Du, M. H. Unconventional Superconductivity with a Sign Reversal in the Order Parameter of $LaFeAsO_{1-x}F_x$. *Phys. Rev. Lett.* **101**, 057003 (2008).
5. Kuroki, K. *et al.* Unconventional Pairing Originating from the Disconnected Fermi Surfaces of Superconducting $LaFeAsO_{1-x}F_x$. *Phys. Rev. Let.* **101**, 087004 (2008).
6. Kontani, H. & Onari, S. Orbital-Fluctuation-Mediated Superconductivity in Iron Pnictides: Analysis of the Five-Orbital Hubbard-Holstein Model. *Phys. Rev. Lett.* **104**, 157001 (2010).
7. Yanagi, Y., Yamakawa, Y. & Ono, Y. Two types of *s*-wave pairing due to magnetic and orbital fluctuations in the two-dimensional 16-band *d-p* model for iron-based superconductors. *Phys. Rev. B* **81**, 054518 (2010).
8. Lu, D. H. *et al.* Electronic structure of the iron-based superconductor LaOFeP. *Nature* **455**, 81 (2008).
9. Kondo, T. *et al.* Momentum Dependence of the Superconducting Gap in $NdFeAsO_{0.9}F_{0.1}$ Single Crystals Measured by Angle Resolved Photoemission Spectroscopy. *Phys. Rev. Lett.* **101**, 147003 (2008).
10. Nishi, I. *et al.* Angle-resolved photoemission spectroscopy study of $PrFeAsO_{0.7}$: Comparison with LaFePO. *Phys. Rev. B* **84**, 014504 (2011).
11. Hajiri, T. *et al.* Three-dimensional electronic structure and interband nesting in the stoichiometric superconductor LiFeAs. *Phys Rev. B* **85**, 094509 (2012).
12. Nakayama, K. *et al.* Angle-Resolved Photoemission Spectroscopy of the Iron-Chalcogenide Superconductor $Fe_{1.03}Te_{0.7}Se_{0.3}$: Strong Coupling Behavior and the Universality of Interband Scattering. *Phys. Rev. Lett.* **105**, 197001 (2010).
13. Qian, T. *et al.* Quasinested Fe orbitals versus Mott-insulating V obitals in superconducting $Sr_2VFeAsO_3$ as seen from angle-resolved photoemission. *Phys. Rev. B* **83**, 140513 (2011).
14. Zhang, Y. *et al.* Nodeless superconducting gap in $A_xFe_2Se_2$ (A = K,Cs) revealed by angle-resolved photoemission spectroscopy. *Nature Mater.* **10**, 273 (2011).
15. Qian, T. *et al.* Absence of a Holelike Fermi Surface for Iron-Based $K_{0.8}Fe_{1.7}Se_2$ Superconductor Revealed by Angle-Resolved Photoemission Spectroscopy. *Phys. Rev. Lett.* **106**, 187001 (2011).
16. Mou, D. X. *et al.* Distinct Fermi surface topology and nodeless superconducting gap in a $Tl_{0.58}Rb_{0.42}Fe_{1.72}Se_2$ superconductor. *Phys. Rev. Lett.* **106**, 107001 (2011).
17. Ding, H. *et al.* Observation of Fermi-surface-dependent nodeless superconducting gaps in $Ba_{0.6}K_{0.4}Fe_2As_2$. *Europhys. Lett.* **83**, 47001 (2008).
18. Terashima, K. *et al.* Fermi surface nesting induced strong pairing in iron-based superconductors. *Proc. Natl. Acad. Sci. U.S.A.* **106**, 7330 (2009).
19. Zhang, Y. *et al.* Orbital characters of bands in the iron-based superconductor $BaFe_{1.85}Co_{0.15}As_2$. *Phys. Rev. B* **83**, 054510 (2011).
20. Fink, J. *et al.* Electronic structure studies of $BaFe_2As_2$ by angle-resolved photoemission apectroscopy. *Phys. Rev. B* **79**, 155118 (2009).
21. Yoshida, T. *et al.* Two-Dimensional and Three-Dimensional Fermi Surfaces of superconducting $BaFe_2(As_{1-x}P_x)_2$ and Their Nesting Properties Revealed by Angle-Resolved Photoemission Spectroscopy. *Phys. Rev. Lett.* **106**, 117001 (2011).
22. Aswartham, S. *et al.* Hole doping in $BaFe_2As_2$: The case of $Ba_{1-x}Na_xFe_2As_2$ single crystals. *Phys. Rev. B* **85**, 224520 (2012).
23. Evtushinsky, D. V. *et al.* Electronic band structure and momentum dependence of the superconducting gap in $Ca_{1-x}Na_xFe_2As_2$ from angle-resolved photoemission spectroscopy. *Phys. Rev. B* **87**, 094501 (2013).
24. Zhang, Y. *et al.* Out-of-Plane Momentum and Symmetry-Dependent Energy Gap of the Pnictide $Ba_{0.6}K_{0.4}Fe_2As_2$ Superconductor Revealed by Angle-Resolved Photoemission Spectroscopy. *Phys. Rev. Lett.* **105**, 117003 (2010).
25. Xu, Y.-M. *et al.* Observation of a ubiquitous three-dimensional superconducting gap function in optimally doped $Ba_{0.6}K_{0.4}Fe_2As_2$. *Nat. Phys.* **7**, 198 (2011).
26. Liu, C. *et al.* Importance of the Fermi-surface topology to the superconducting state of the electron-doped pnictide $Ba(Fe_{1-x}Co_x)_2As_2$. *Phys. Rev. B* **84**, 020509 (2011).
27. Malaeb, W. *et al.* Three-Dimensional Electronic Structure of Superconducting Iron Pnictides Observed by Angle-Resolved Photoemission Spectroscopy. *J. Phys. Soc. Jpn.* **78**, 123706 (2009).
28. Kito, H., Eisaki, H. & Iyo, A. Superconductivity at 54 K in F-Free $NdFeAsO_{1-y}$. *J. Phys. Soc. Jpn.* **77**, 063707 (2008).
29. Kudo, K. *et al.* Emergence of superconductivity at 45 K by lanthanum and phosphorus co-doping of $CaFe_2As_2$. *Sci. Rep.* **3**, 1478 (2013).
30. Krellner, C. *et al.* Magnetic and structural transitions in layered iron arsenide systems: AFe_2As_2 versus *R*FeAsO. *Phys. Rev. B* **78**, 100504 (2008).
31. Canfield, P. C. *et al.* Structural, magnetic and superconducting phase transitions in $CaFe_2As_2$ under ambient and applied pressure. *Physica C* **469**, 404–412 (2009).
32. Kondo, T. *et al.* Unexpected Fermi-surface nesting in the pnictide parent compounds $BaFe_2As_2$ and $CaFe_2As_2$ revealed by angle-resolved photoemission spectroscopy. *Phys. Rev. B* **81**, 060507 (2010).
33. Huang, Y.-B. *et al.* Experimental investigation of the electronic structure of $Ca_{0.83}La_{0.17}Fe_2As_2$. *Chinese Phys. Lett.* **30**, 017402 (2013).
34. Usui, H., Suzuki, K. & Kuroki, K. Least momentum space frustration as a condition for a 'high T_c sweet spot' in iron-based superconductors. *Supercond. Sci. Technol.* **25**, 084004 (2012).
35. Suzuki, K. *et al.* Key role of prioritized diagonal motion of electrons in the iron-based superconductors. http://arxiv.org/abs/1311.2413v1 (2013).
36. Analytis, J. G., Chu, J.-H., McDonald, R. D., Riggs, S. C. & Fisher, I. R. Enhanced Fermi-Surface Nesting in Superconducting $BaFe_2(As_{1-x}P_x)_2$ Revealed by the de Haas-van Alphen effect. *Phys. Rev. Lett.* **105**, 207004 (2010).
37. Drotziger, S. *et al.* Pressure versus Concentration Tuning of the Superconductivity in $Ba(Fe_{1-x}Co_x)_2As_2$. *J. Phys. Soc. Jpn.* **79**, 124705 (2010).
38. Rotter, M., Tegel, M. & Johrendt, D. Superconductivity at 38 K in the Iron Arsenide $(Ba_{1-x}K_x)Fe_2As_2$. *Phys. Rev. Lett.* **101**, 107006 (2008).

Acknowledgments

We acknowledge S. Nagira and H. Fujiwara for technical assistance and Y. Inada for Laue x-ray diffraction experiments. We thank K. Kuroki for the valuable discussions. We also thank A. Ino and R. Yoshida for their ARPES data analysis program. Polarization dependent ARPES experiments at HSRC were performed with the approval of HSRC (Proposal No. 13-A-4). ARPES experiments at the Photon Factory were approved by the Photon Factory Program Advisory Committee (Proposal No. 2011G086). Part of this work was performed at the Advanced Science Research Center at Okayama University. This work was partially supported by MEXT KAKENHI Grant Number 20102003 and JSPS Grant Number 25400372. This work was also partially supported by the Funding Program for

World-Leading Innovative R&D in Science and Technology (FIRST program) from JSPS and the program for promoting the enhancement of research universities from MEXT.

Author contributions

M.S., T.I., K.T., T.J. and J.S. performed ARPES experiments. K.O., H.K., M.A., K.S., H.N. and M.T. supported Synchrotron ARPES experiments. M.S. analyzed data. M.S. and T.Y. designed experiments. K.I., K.K. and M.N. synthesized single crystals. M.S., K.K., M.N., T.M., T.W., Y.M. and T.Y. discussed the results and M.S. and T.Y. wrote the manuscript.

Additional information

Supplementary information accompanies this paper at http://www.nature.com/scientificreports

Competing financial interests: The authors declare no competing financial interests.

How to cite this article: Sunagawa, M. *et al*. Characteristic two-dimensional Fermi surface topology of high-T_c iron-based superconductors. *Sci. Rep.* **4**, 4381; DOI:10.1038/srep04381 (2014).